

INTERACTION OF LASER RADIATION WITH MATTER https://doi.org/10.1070/QEL17598

Measurements of the absolute intensities of spectral lines of Kr, Ar, and O ions in the wavelength range of 10–18 nm under pulsed laser excitation

A.V. Vodop'yanov, S.A. Garakhin, I.G. Zabrodin, S.Yu. Zuev, A.Ya. Lopatin, A.N. Nechay, A.E. Pestov, A.A. Perekalov, R.S. Pleshkov, V.N. Polkovnikov, N.N. Salashchenko, R.M. Smertin, B.A. Ulasevich, N.I. Chkhalo

Abstract. **We have measured the absolute intensities of the spectral lines of Kr, Ar, and O ions (CO_2 gas), which are of interest for reflectometry, microscopy, and lithography in the wavelength range of 10–18 nm. We have used pulsed excitation by an Nd:YAG laser with an output wavelength $\lambda = 1064$ nm, a pulse energy of 0.8 J, a pulse duration of 5.2 ns and a pulse repetition rate of 10 Hz. The targets are formed during gas outflow through a pulsed supersonic conical nozzle for an inlet gas pressure of 3.5 bar. A spectrometer based on X-ray multilayer mirrors and its calibration procedure are described in detail. The absolute intensities of the spectral lines of Kr IX ($\lambda = 11.5$ nm; number of photons: $N = 9.3 \times 10^{12}$ photons pulse^{-1}), Ar VIII ($\lambda = 13.84$ nm, $N = 3 \times 10^{12}$ photons pulse^{-1}), and O VI ($\lambda = 12.98$ nm, $N = 5.17 \times 10^{12}$ photons pulse^{-1}). The results are compared with the data obtained for Xe ions under the same experimental conditions at the same wavelengths.**

Keywords: *extreme UV radiation, emission spectra, laser-produced spark, spectrometer, plasma, X-ray multilayer mirror.*

1. Introduction

At present, in connection with the progress in the development of radiation sources and optical elements, research is actively pursued in the field of soft X-ray (SXR) and extreme UV (EUV) radiation, where lithography and microscopy are the most promising areas. The key element in the development of both lines is a point source of SXR and EUV radiation. Such sources should have a suitable emission spectrum in the selected wavelength range, a high radiation intensity, good stability, and a high efficiency of conversion of pump radiation into SXR and EUV radiation.

For use in lithography, as well as in related research, many source designs have been proposed, differing both in average output power and in the physical principle of producing multiply charged plasma ions radiating in the requisite wavelength range. The most widespread are laser-plasma sources (LPS's) based on plasma produced by high-power laser pulse irradiation of a solid tin [1] or tin-containing [2] target and generating radiation in the vicinity of $\lambda = 13.5$ nm with a high efficiency. Research is also underway in the field of X-ray multilayer optics and radiation sources for wavelengths of 11.2, 10.5, and 6.7 nm [3–7]. The use of shorter wavelengths makes it possible to improve the resolution of lithographic facilities.

The main advantages of sources based on solid targets are a high average power and a high laser-to-short-wavelength radiation conversion efficiency, which amounts to 6%–7% in the spectral band of width equal to 2% of the fundamental wavelength in the vicinity of $\lambda = 13.5$ nm [8]. The main disadvantage of such sources is heavy contamination of structural elements and optics with target erosion products, which requires the use of complex and expensive systems to eliminate this effect [9, 10]. As a result, these sources can only be used in mass production. For this reason, an active search is underway for alternative sources using gas-jet [11–14], cluster [15–17], frozen gas [18, 19], and liquid [20, 21] targets. The main advantage of such targets over solid-state targets is the minimisation of contamination of optical elements of the setup. Despite a lot of works on gas-jet targets, most of the research concerns the measurement of spectra and the identification of their lines, as well as the influence of source parameters on the relative line intensities. There are a limited number of works that give the absolute line intensities. For the spectral regions near $\lambda = 13.5$ and 11 nm, mention should be made of the study of xenon-based sources [22–24]. For the region 10–11 nm, the absolute intensities of krypton radiation, as far as we know, were presented only in work [25]. For the region about $\lambda = 6.7$ nm, the laser-to-X-ray radiation conversion efficiency was measured in Ref. [7]. In connection with the development of laboratory microscopy, the conversion efficiencies for nitrogen, argon, and various alcohols were measured in the so-called water transparency window ($\lambda = 2.3$–4.4 nm) [26–30].

The aim of this work is to search for the most promising gas targets and spectral lines for making LPS's intended for EUV lithography and microscopy in the 12.4–14 nm domain, where multilayer optics based on Mo/Si structures are used, and in the 11.1–12.4 nm domain, where beryllium-based multilayer structures (Ru/Be and Mo/Be) exhibit the highest reflection coefficients [31, 32]. Since the replacement of expensive xenon used for lithographic and microscopic tasks in the 10–18 nm spectral range is a topical problem, we investigated the spectra of available and easy-to-use Kr, Ar, and CO_2 gases.

Considerable emphasis is also placed on a responsivity-calibrated automated broadband spectrometer based on

A.V. Vodop'yanov Institute of Applied Physics, Russian Academy of Sciences, ul. Ul'yanova 46, 603950 Nizhny Novgorod, Russia;
S.A. Garakhin, I.G. Zabrodin, S.Yu. Zuev, A.Ya. Lopatin, A.N. Nechay, A.E. Pestov, A.A. Perekalov, R.S. Pleshkov, V.N. Polkovnikov, N.N. Salashchenko, R.M. Smertin, B.A. Ulasevich, N.I. Chkhalo Institute for Physics of Microstructures, Russian Academy of Sciences, ul. Akademicheskaya 7, Afonino, Kstovskii district, 603087 Nizhny Novgorod region; e-mail: nechay@ipm.sci-nnov.ru

Received 25 February 2021; revision received 8 June 2021
Kvantovaya Elektronika **51** (8) 700–707 (2021)
Translated by E.N. Ragozin

X-ray multilayer mirrors. The developed spectrometer makes it possible to measure the radiation intensity in absolute units in the range of 7–32 nm. When using short-period W/B_4C multilayer mirrors [33], the working range can be extended to the short-wavelength region down to 1.35 nm. With the use of Al/Sc multilayer mirrors [34], the range may be extended to the long-wavelength region up to 70 nm. Furthermore, the spectrometer design makes it easy to integrate it for measurements with existing equipment and vacuum chambers.

This paper presents the results of studies of the emission spectra of Ar, Kr, and CO_2 gas targets under pulsed laser excitation and the absolute radiation intensities at wavelengths of 11.5 nm (Kr), 13.84 nm (Ar), and 12.98 nm (CO_2), which made it possible to choose the optimal wavelengths for upgrading the EUV stand of the lithographer [35] and the microscope currently being developed [36].

2. Experiment scheme and metrological equipment

The intensity of emission lines was measured on a setup intended for studying the emission spectra of gas and atomic-cluster targets. The setup is schematically shown in Fig. 1.

To produce gas-jet targets, a supersonic conical nozzle was used (nozzle throat diameter: $d_{cr} = 450$ μm; nozzle length: $L = 5$ mm; cone half-angle: 5°) operating in a pulsed mode. The residual pressure in the chamber was $\sim 10^{-2}$ Pa. The excitation source was the radiation of a pulsed Nd:YAG laser ($\lambda = 1064$ nm; pulse energy and duration: 0.8 J and 5 ns, respectively; pulse repetition rate: 10 Hz). The principles of construction and operation of the facility, which was used for carrying out the research, are described in greater detail in Ref. [37].

Initially, the emission spectra were recorded using an RSM-500 grazing incidence spectrometer-monochromator. The instrument operates as follows: the radiation of the laser spark is incident on the entrance mirror of the spectrometer-monochromator with a radius of curvature of 4 m and then on the entrance slit of the instrument. The radiation is then decomposed into a spectrum by a spherical diffraction grating with a radius of curvature of 3 m, passes through the collimator slit, the exit slit, and illuminates the photocathode coated with a CsI layer. The electrons escaping from the photocathode are detected using a chevron assembly of two microchannel plates. In the course of spectral measurements, the exit slit and the diffraction grating of the spectrometer-monochroma-

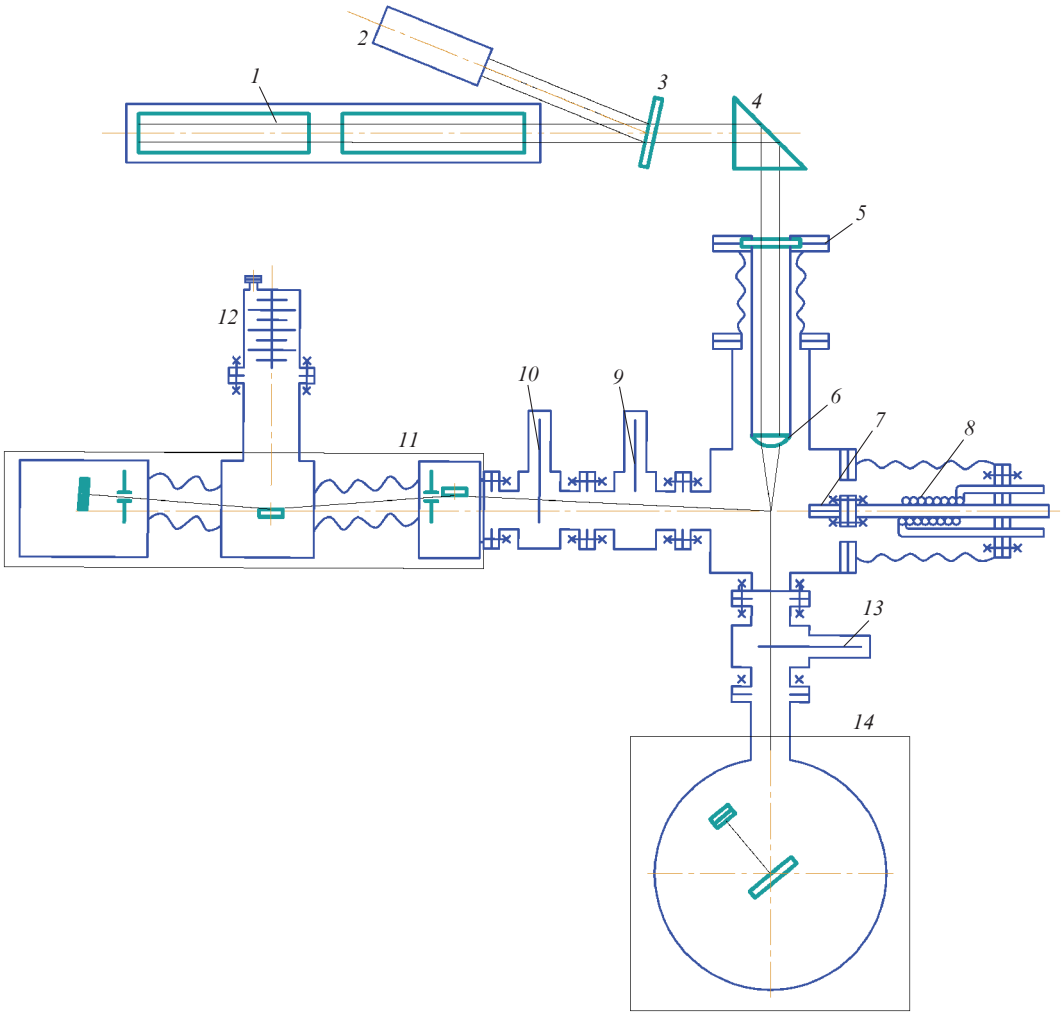

Figure 1. Schematic of the facility: (*1*) laser; (*2*) laser radiation power sensor; (*3*) beam splitter; (*4*) prism; (*5*) optical input; (*6*) lens; (*7*) nozzle; (*8*) heat exchanger; (*9*) vacuum gate; (*10*) film filter; (*11*) RSM-500 spectrometer-monochromator; (*12*) turbomolecular pump; (*13*) entrance film filter; (*14*) spectrometer for measuring absolute radiation intensities.

tor move in accordance with the focusing conditions along the Rowland circle. The SXR/EUV radiation is recorded in a pulsed mode. The detection system is triggered by a clock pulse coming from the laser control system.

The spectral resolution of the spectrometer-monochromator was determined from the zero-order half-width and from the narrow spectral lines of oxygen ions and was 0.04 nm. For the grating and mirror used, the wavelength range under investigation was 3–20 nm. The spectral studies carried out with the RSM-500 make it possible to determine the position of high-intensity spectral lines, whose absolute intensity was measured by another instrument described below.

To measure the absolute radiation intensities, we developed a special-purpose absolute-calibrated spectrometer, whose schematic with the designations of the main elements and the position of the radiation source is depicted in Fig. 2. In contrast to the quantometer calibrated in sensitivity, wavelength, and bandwidth, described in Ref. [38] and used as a secondary standard for determining the radiation characteristics of EUV lithography sources, the newly developed spectrometer permits scanning over the spectrum.

The body of the spectrometer is a stainless-steel cylinder 200 mm in diameter. On the top cover there is a window for visual observation of the $\varphi - 2\varphi$-goniometer operation. When recording the radiation spectra, the window is closed with a special cover to eliminate the detector illumination. On the bottom cover there are two RMG-7 connectors for connecting a detector and a stepper motor to the control unit. Inside the housing there is a $\varphi - 2\varphi$-goniometer, in which a stepper motor is used for the drive. The 22°–75° range of grazing incidence angles accounts for 2400 motor steps. The minimum angle was chosen so as to depart from the angle of total external reflection of the multilayer mirror. The maximum angle is limited by the size of the spectrometer chamber and by the incident radiation shielding by the detector assembly. The mechanical positioning accuracy is much higher than the spectral resolution of the spectrometer. One step of the goniometer in the worst case corresponds to 0.006 nm for the instrument resolution of ~0.2 nm at best. The spectrometer is connected to the vacuum chamber through an CF40 flange. The weight of the instrument is ~10 kg.

The instrument works as follows. The radiation of the laser spark (*1*) passes through the entrance free-standing film filter (*2*) and illuminates the X-ray multilayer mirror (XMM) (*3*) arranged relative to the incident beam at a certain angle, called the grazing angle. The XMM is used in this spectrometer as a dispersing element. In accordance with Wulff–Bragg's condition, the mirror reflects the radiation with a certain wavelength, which passes through a round aperture (*4*) with a diameter of 4 mm, which is used to improve the spectral resolution of the instrument by reducing the angular divergence of the detected radiation. On passing through the free-standing film filter (*5*), it arrives at the detector (*6*). Spectral scanning is performed by rotating (by an angle φ) the XMM relative to the incident beam, while the detector is rotated relative to the incident beam by the doubled angle (2φ). The mirror and detector are rotated by a stepper motor due to a gear transmission. The recorded signal is displayed on the computer screen and stored in the form of a numerical table. In the operation of the instrument, the total distance from the laser spark to the 4-mm aperture was 480 mm. Therefore, the laser spark radiation was recorded at a solid angle of 5.45×10^{-5} sr.

3. Method for calculating the number of photons in the spectral emission band

In our experiment, the recorded detector voltage, induced by one laser pulse, can be determined by the formula

$$V = \int_0^\infty \frac{\Omega\beta^2}{4\pi\alpha} E(\lambda)\delta(\lambda)T^2(\lambda)R(\lambda)\mathrm{d}\lambda, \qquad (1)$$

where V (in V) is the voltage recorded by the detector; α (in C V^{-1}) is the amplifier responsivity; β is the transmittance of the filter support mesh; Ω (in sr) is the solid angle in which the radiation is recorded by the detector; E (in J nm^{-1}) is the spec-

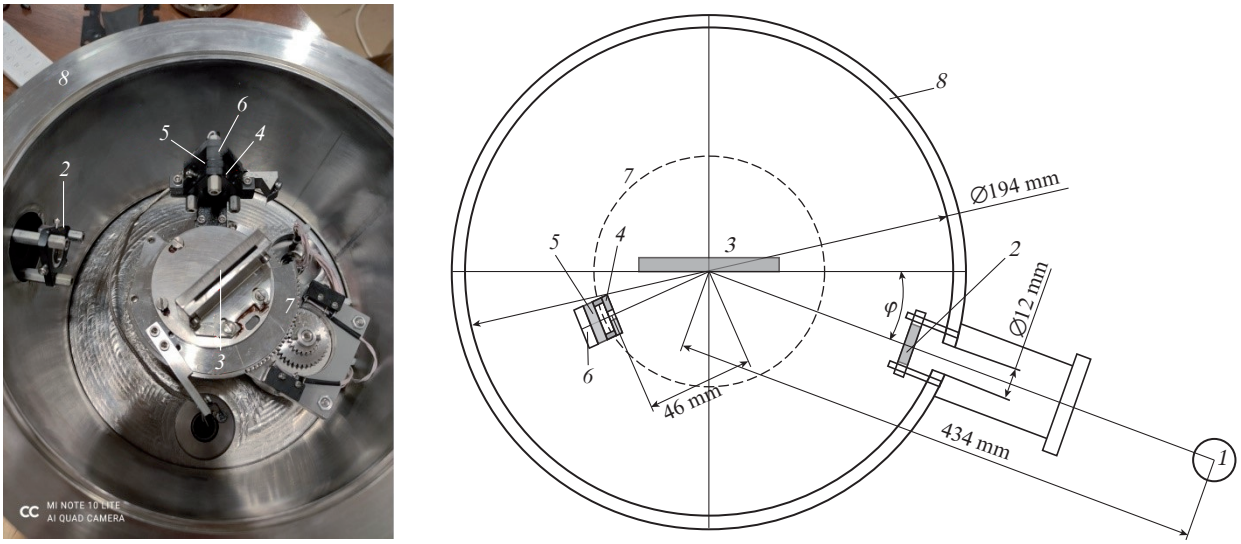

Figure 2. Photograph of the spectrometer absolute-calibrated and its schematic: (*1*) laser spark domain; (*2*) entrance free-standing film filter; (*3*) X-ray multilayer mirror; (*4*) aperture in front of the detector; (*5*) free- standing film filter of the detector; (*6*) detector; (*7*) $\varphi-2\varphi$-goniometer; (*8*) instrument housing.

tral density of the plasma radiation energy; δ (in C J^{-1}) is the detector responsivity; $T(\lambda)$ is the transmittance of the free-standing film filter; and $R(\lambda)$ is the reflection coefficient of the XMM. Taking into account the resonance nature of reflection from multilayer mirrors, it is sufficient to carry out integration in the range $\pm 3\Delta\lambda_{1/2}$, where $\Delta\lambda_{1/2}$ is the width of the spectral reflection coefficient of the multilayer mirror at half maximum. The spectral dependences of the filter transmission and detector responsivity within the reflection band of such a mirror are smooth functions; they can be taken outside the integral sign and replaced by their values at the resonant wavelength λ_{res}. The exceptions are the near-edge transmission regions of the filters and the Si L-edge of absorption (λ = 12.4 nm), where a small jump in the detector sensitivity is observed. In the case of narrow, sufficiently isolated spectral lines, it can be assumed that practically all the energy is contained in the region near the wavelength λ_{lin}. Consequently, the energy E_{lin} confined in the emission line and the number of photons N_{lin} in it can be defined by the expressions

$$E_{lin} = \frac{4\pi\alpha V}{\Omega\delta T^2 R\beta^2}, \quad (2)$$

$$N_{lin} = E_{lin}\frac{\lambda_{lin}}{hc}. \quad (3)$$

For the spectral range studied by us, the amplifier responsivity is $\alpha = 10^{-11}$ C V^{-1}, coefficient β = 0.8, angle $\Omega = 5.45 \times 10^{-5}$ sr, and detector responsivity δ = 0.25 C J^{-1}. The numerical values of transmittance and reflectance are discussed in detail in the next section.

4. Calibration of the quantum efficiency of the spectrometer

To determine the absolute line intensities, it is necessary to calibrate all values included in expressions (2) and (3). In this work, we used three types of multilayer mirrors based on Mo/B$_4$C, Mo/Be, and Be/Si/Al structures. The main characteristics of the mirrors are listed in Table 1.

Table 1. Characteristics of the XMMs in use.

Structure	Period/nm	Number of layers	Operating wavelength range/nm
Mo/B$_4$C	6.5	60	6.5–11.9
Mo/Be	9.83	50	10–18
Be/Si/Al	18.2	40	17–32

Figures 3 and 4 show the wavelength dependences of the reflection coefficients and spectral resolution of the multilayer mirrors in use. The choice of multilayer mirror designs, in particular the new Be/Si/Al system [39], is due to the best combination of reflection coefficients and spectral selectivity with long-term stability of X-ray optical characteristics. The reflection coefficients were measured using the laboratory reflectometers described in Refs [40, 41].

When calculating the reflective characteristics of multilayer mirrors, we used the film thicknesses, the interface widths and shapes obtained from the data of joint reconstruction of X-ray reflection curves at several wavelengths using the technique described in Ref. [42].

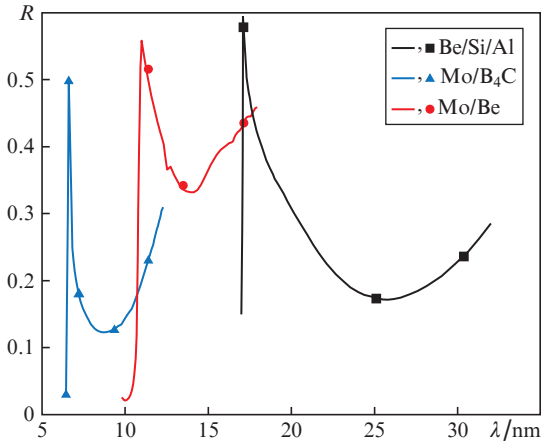

Figure 3. Wavelength dependences of the reflection coefficients of the XMMs in use. Solid curves are calculated dependences, and points are measurement results.

In practice, because of the finite distance between the radiation source and the spectrometer, which leads to the angular divergence of the recorded radiation beam, the spectral reflection band of multilayer mirrors broadens. Therefore, Fig. 4 also shows the results of measuring the width at half maximum of the reflection curve observed when narrow emission lines of oxygen ions were recorded with the XMM spectrometer (denoted by rhombuses). One can see that the resolution is mainly determined by the width at half maximum of the XMM reflection curve. As expected, the resolution obtained in the experiments is somewhat lower than the calculated one, and later this was taken into account in the interpretation of experimental data.

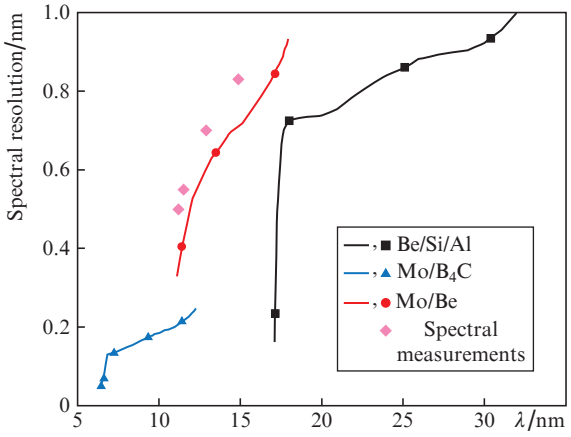

Figure 4. Wavelength dependences of the spectral resolution of the XMMs in use. Solid curves are calculated dependences, and points are measurement results.

To suppress background noise and the higher orders of reflection of multilayer mirrors, three types of thin-film absorption filters were used: Mo/C, Mo/Be, and Al. Figure 5 shows the spectral dependences of the transmission coefficients of these filters.

Film filters have the following structure. Al filter: $MoSi_2$ (2.5 nm)/Al (150 nm)/$MoSi_2$ (2.5 nm); Mo/Be filter: $MoSi_2$

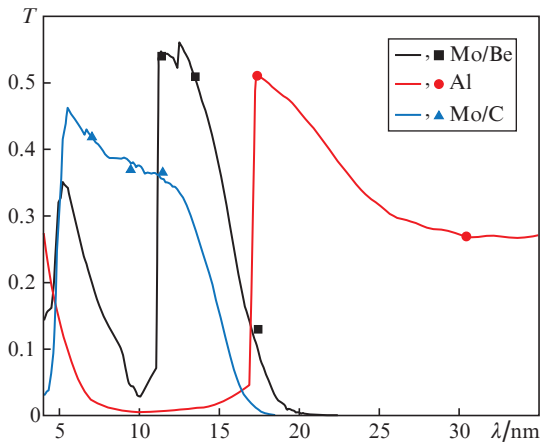

Figure 5. Spectral dependences of the transmittance of the film filters in use. Solid curves are calculated dependencies, and points are measurement results.

(2.5 nm)/Mo (2 nm) (Be (3 nm), Mo (2 nm)) × 30 periods/$MoSi_2$ (2.5 nm); Mo/C filter: C (0.7 nm)/(Mo (2 nm), C (0.7 nm)) × 60 periods. The filter characteristics are described in more detail in Refs [43, 44].

To record EUV radiation, the spectrometer has an SPD-100UV silicon photodiode absolute-calibrated on the BESSY II synchrotron. The sensitive photodiode area is of the form of a square with a side of 10 mm. The photodiode responsivity is ~0.25 C J^{-1} in the spectral range under our study. The manufacturing technology, design, and characteristics of the photodiode are described in more detail in Ref. [45].

The stepper motor and the detector are connected to the spectrometer control unit, which permits recording spectra in continuous and pulsed modes (with external synchronisation). The detector signal amplifier is integrated into the control unit and can operate in three amplification ranges. The control unit works automatically with data output to the computer.

Taking into account the measurement errors of the reflectivity of the mirrors, the filter transmittances, the detector responsivity and geometric parameters, as well as the statistical fluctuations of the recorded intensity, we estimate the measurement error of the absolute line intensities at ±10%, which is quite sufficient for the majority of applications.

5. Experimental results

5.1. Krypton

Krypton is a heavy inert gas characterised by a high intensity of radiation when used as a target for an LPS. The krypton spectrum contains a large number of rather bright lines.

Figure 6 shows the emission spectra of krypton in the range 10–18 nm, measured using an XMM-based spectrometer and an RSM-500 grating spectrometer-monochromator under the same experimental conditions. The krypton pressure at the nozzle inlet was 3.5 bar.

In the krypton spectrum (Fig.6a), a band with a maximum at $\lambda \approx 11.5$ nm is clearly pronounced. This band corresponds to the lines of KrIX ions at wavelengths of 11.49 and 11.57 nm. The lines are not resolved in the spectrum due to the fact that the resolution of the XMM-based spectrometer in this region is 0.52 nm. A small maximum observed about $\lambda = 12.1$ nm

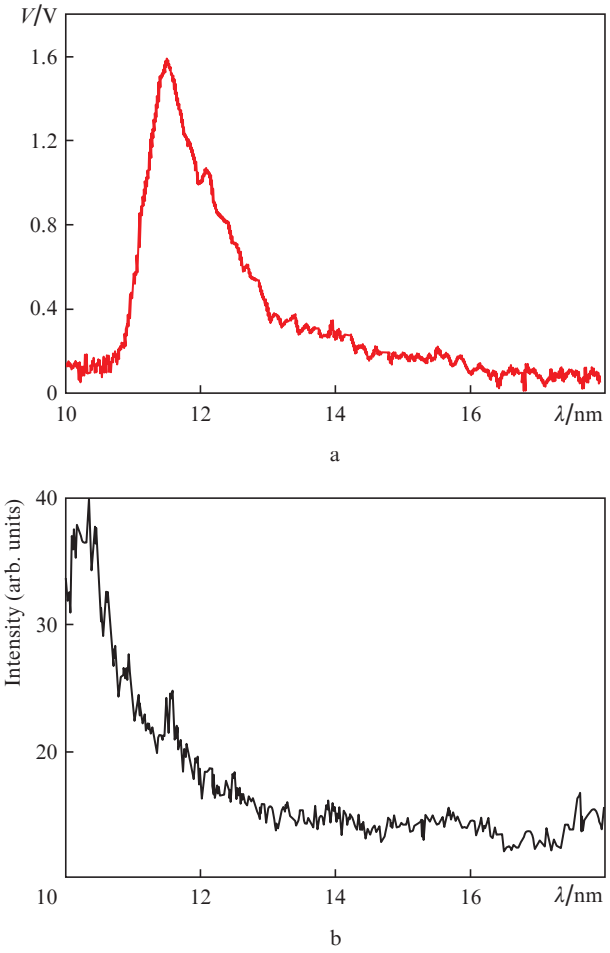

Figure 6. Emission spectra of krypton recorded using (a) our XMM-based spectrometer and (b) an RSM-500 spectrometer-monochromator.

corresponds to the $\lambda = 12.15$ nm line of KrVIII. The spectra recorded with the RSM-500 spectrometer were identified using the data of Refs [46–48].

A sharp decrease in the magnitude of the recorded signal when using the XMM-based spectrometer for wavelengths less than 11 nm is explained by the fact that the K-absorption edge of Be is located in this spectral region, and therefore the reflectivity and transmission of multilayer mirrors and Mo/Be filters are greatly impaired (see Fig. 3).

The measured intensity of the emission band was used to calculate the laser-spark radiation energy (and the number of photons) into a full solid angle in the spectral band 11.5 ± 0.11 nm under single laser pulse irradiation. The calculation results are presented in Table 2.

5.2. Argon

Due to its sufficiently large atomic mass and availability, argon is a promising gas for use as an LPS target. Figure 7 shows the emission spectra of argon in the range 10–18 nm recorded using the XMM-based spectrometer and the RSM-500 grating spectrometer-monochromator under the same experimental conditions. The argon pressure at the nozzle inlet was 3.5 bar.

The argon spectrum contains bands with maxima at $\lambda \approx$ 12, 13.8, and 15.8 nm. The first band corresponds to two lines

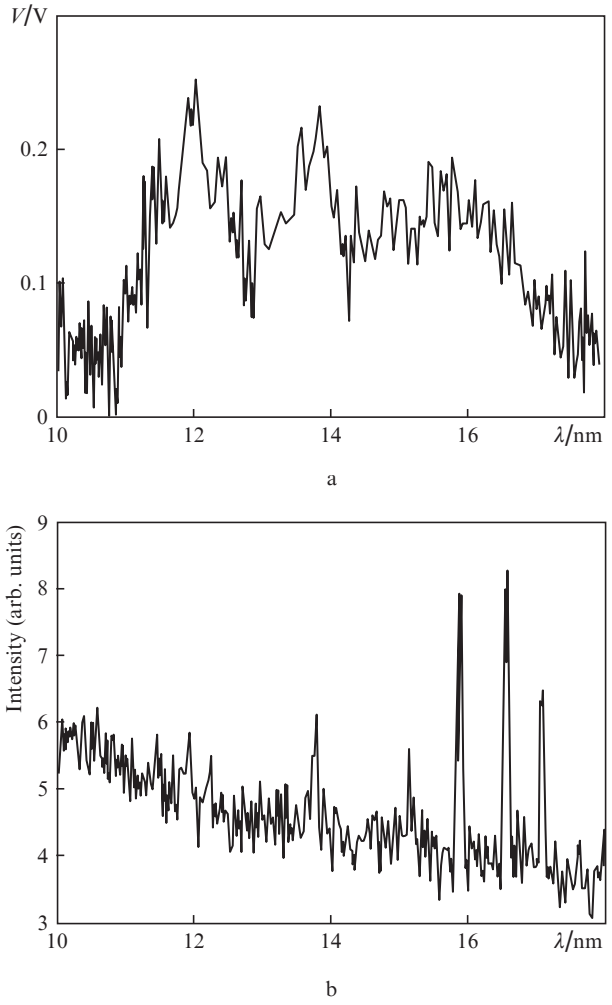

Figure 7. Argon emission spectra recorded with (a) the XMM-based spectrometer and (b) the RSM-500 spectrometer-monochromator.

of ArVIII ions at λ = 12 and 12.3 nm, the second, to the ArVIII lines at λ = 13.84 nm, and the third, to three high-intensity ArVIII lines at λ = 15–17 nm. The low intensity of this band is explained by a significant decrease in the transmittance of Mo/Be film filters at wavelengths exceeding 15 nm (see Fig. 5). The resolution of the absolute-calibrated spectrometer is about 0.6 nm at $\lambda \approx 12$ nm and about 0.76 nm at $\lambda \approx 13.8$ nm. The spectra recorded with the RSM-500 spectrometer was identified using the data of Refs [46, 49, 50].

A sharp decrease in the magnitude of the recorded signal when using the XMM-based spectrometer for wavelengths shorter than 11 nm is explained by the presence of the K-absorption edge of Be, which is part of the multilayer mirror and filter.

The measured intensity of the emission band was used to calculate the radiation energy (and the number of photons) of the laser spark into a full solid angle in the spectral band 13.84 ± 0.14 nm. The calculation result is shown in Table 2.

5.3. CO_2

Carbon dioxide is a rather heavy molecular gas. It is characterised by a pronounced line emission spectrum in the SXR and EUV wavelength ranges. The line intensities of the spectrum are quite high. Therefore, this gas is a promising gas target for an LPS.

Figure 8 shows the emission spectra of carbon dioxide in the 10–18 nm range recorded using the XMM-based spectrometer and the RSM-500 grating spectrometer-monochromator under the same experimental conditions. The CO_2 pressure at the nozzle inlet was 3.5 bar.

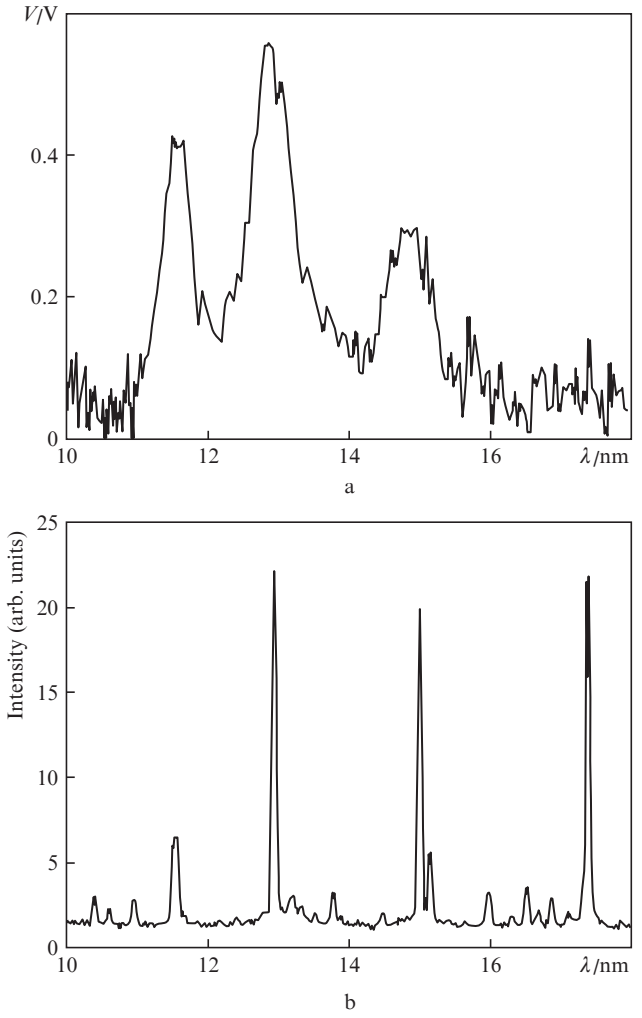

Figure 8. CO_2 emission spectra recorded with (a) the XMM-based spectrometer and (b) the RSM-500 spectrometer-monochromator.

The spectrum of carbon dioxide contains three bands with maxima at $\lambda \approx 11.6$, 12.98, and 15.05 nm. The first band corresponds to the OVI ion line at λ = 11.64 nm, the second to the OVI ion line at λ = 12.98 nm, and the third to the high-intensity OVI ion line at λ = 15.01 nm and the less intense OV ion line at λ = 15.15 nm. The significant difference in the intensities of these lines recorded with the XMM-based spectrometer and the RSM-500 spectrometer-monochromator is explained by the nonuniformity of the reflection and transmission coefficients of multilayer mirrors and Mo/Be film filters. The high-intensity line of OVI ions at λ = 17.3 nm is strongly suppressed when recording with the XMM-based spectrometer due to a significant decrease in the transmittance of Mo/Be film filters in this spectral region. The resolution of the XMM-

based spectrometer is about 0.54 nm in the $\lambda \approx 11.6$ nm region, about 0.7 nm in the $\lambda \approx 12.98$ nm region, and about 0.82 nm in the $\lambda \approx 15.05$ nm region. The spectra recorded with the RSM-500 spectrometer were identified using the data of Ref. [46].

The sharp lowering of the recorded signal when using the XMM-based spectrometer for wavelengths shorter than 11 nm is explained by the presence of the K absorption edge of Be, which is part of the multilayer mirror and filter.

The measured intensity of the emission band was used to calculate the radiation energy (and the number of photons) of the laser spark into a full solid angle in the spectral band 12.98 ± 0.13 nm. The calculation result is shown in Table 2.

6. Discussion of results and main conclusions

In the course of the research, we determined the radiation energies at wavelengths of 13.84 nm (Ar), 11.5 nm (Kr), and 12.98 nm (CO_2). The data obtained are collected in Table 2.

Table 2. Absolute radiation intensities of Ar, Kr, and CO_2.

Target	Wavelength /nm	Radiation energy /10^{-5} J pulse^{-1}	Number of photons /10^{12} photons pulse^{-1}
Kr	11.5 ± 0.11	16	9.3
CO_2	12.98 ± 0.13	7.9	5.2
Ar	13.84 ± 0.14	4.4	3

It is interesting to compare them with similar data for xenon (Table 3). To this end, the absolute radiation energies were calculated using a xenon target excited by laser radiation in the same spectral ranges. The calculation was carried out using the data borrowed from Ref. [22]. The radiation intensities were estimated for a xenon target with the following parameters. Distance from the nozzle exit: 0.5 mm; pressure at the nozzle inlet: 2.5 bar. The gas jet formation system (valve and nozzle) and the gas target excitation system (laser, focusing lens) are completely similar to those described in this paper. In Ref. [22], the maximum conversion of the laser radiation energy into the radiation energy of the laser spark was observed in the region of 11–18 nm under these conditions.

Table 3. Absolute intensities of xenon radiation.

Target	Wavelength /nm	Radiation energy /10^{-5} J pulse^{-1}	Number of photons /10^{12} photons pulse^{-1}
Xe	11.5 ± 0.11	79	46
Xe	12.98 ± 0.13	9.3	6.1
Xe	13.84 ± 0.14	8.6	6.0

Our results suggest that the absolute intensities of the spectral lines at $\lambda = 11.5$, 12.98, and 13.84 nm when using Ar, Kr and CO_2 targets are comparable to the absolute intensities at the corresponding wavelengths when using a xenon target. Thus, targets based on Ar, Kr, and CO_2 can be used for lithography problems.

Let us formulate the main results of the work:

1. To carry out absolute measurements, an absolute-calibrated XMM-based spectrometer, which operates in the EUV and SXR ranges, has been developed and manufactured. A photodiode absolute-calibrated on the BESSY II synchrotron is used as a detector in the spectrometer. This spectrometer is convenient to install and permits recording spectra without changing the geometry of the optical part of the facility. The device has relatively small dimensions (diameter: 250 mm; height: 150 mm) and weight of ~10 kg. The time taken to record for the entire spectrum does not exceed a few minutes. The sharp changes in the instrument responsivity at the known absorption edges of the materials included in the filters and multilayer mirrors provide spectrum-based wavelength 'self-calibration' of the instrument.

The photon fluxes from the laser spark into a full solid angle were measured in the bands of 11.5 ± 0.11 nm (for Kr), 13.84 ± 0.14 nm (for Ar), and 12.98 ± 0.13 nm (for O). The number of photons $N = 9.3 \times 10^{12}$ photons per pulse for KrIX ($\lambda = 11.5$ nm), 5.2×10^{12} photons per pulse for OVI ($\lambda = 12.98$ nm), and 3×10^{12} photons per pulse for ArVIII ($\lambda = 13.84$ nm). For comparison, the number of photons from xenon ions at the same wavelengths and under the same conditions is estimated as follows: $N = 4.6 \times 10^{13}$ photons per pulse ($\lambda = 11.5$ nm), 6.1×10^{12} photons per pulse ($\lambda = 12.98$ nm) and 6.0×10^{12} photons per pulse. ($\lambda = 13.84$ nm) [22, 51]. Thus, it has been shown that these gases, when used as LPS targets, are comparable in efficiency with xenon.

A significant practical result was the choice of wavelengths and, consequently, gas targets for upgrading the projection lithography stand in the vicinity of $\lambda = 13$ nm and the X-ray microscope being developed. Knowing the efficiency of conversion of laser radiation into the EUV and SXR ranges makes it possible to calculate the intensity of the probe radiation and optimise the experimental conditions.

Acknowledgements. The work was supported by the World-Class Research Centre 'Photonics Centre' under the financial support of the Ministry of Science and High Education of the Russian Federation (Aagreement No. 075-15-2020-906).

References

1. Fomenkov I. et al. *Adv. Opt. Technol.*, **6**, 173 (2017).
2. Abramenko D.B. et al. *Phys.Usp.*, **62**, 304 (2019) [*Usp. Fiz. Nauk*, **189**(3), 323 (2019)].
3. Windt D.L., Gullikson E.M. *Appl. Opt.*, **54**, 5850 (2015).
4. Chkhalo N.I., Salashchenko N.N. *AIP Advances*, **3**(8), 082130 (2013).
5. Wagner C., Harned N. *Nat. Photonics*, **4**, 24 (2010).
6. Otsuka T. et al. *Appl. Phys. Lett.*, **97**(11), 111503 (2010).
7. Chkhalo N.I. et al. *Appl. Phys. Lett.*, **112**(22), 221101 (2018).
8. Fomenkov I.V. et al. *EUV Lithography* (Bellingham, WA, 2018).
9. Elg D.T. et al. *J. Micro/Nanolithogr. MEMS MOEMS*, **14**, 013506 (2015).
10. Bleiner D., Lippert T. *J. Appl. Phys.*, **106**, 123301 (2009).
11. Fiedorowicz H. et al. *Opt. Commun.*, **163**(1-3), 103 (1999).
12. Fiedorowicz H. et al. *Appl. Phys. Lett.*, **62**(22), 2778 (1993).
13. Holburg J. et al. *J. Vac. Sci. Technol. A*, **37**(3), 031303 (2019).
14. Zabrodskii V.V. et al. *Tech. Phys. Lett.*, **40**, 648 (2014) [*Pis'ma Zh. Tekh. Fiz.*, **40**(15), 38 (2014)].
15. Mocek T. et al. *Phys. Rev. E*, **62**(3), 4461 (2000).
16. Ter-Avetisyan S. et al. *J. Appl. Phys.*, **94**(9), 5489 (2003).
17. Parra E. et al. *Phys. Rev. E*, **62**(5), R5931 (2000).
18. Shimoura A. et al. *Appl. Phys. Lett.*, **72**(2), 164 (1998).
19. Shimoura A. et al. *App. Phys. Lett.*, **75**(14), 2026 (1999).
20. De Groot J. et al. *J. Appl. Phys.*, **94**(6), 3717 (2003).
21. Vogt U. et al. *Appl. Phys. Lett.*, **79**(15), 2336 (2001).
22. Chkhalo N.I. et al. *AIP Advances*, **8**(10), 105003 (2018).
23. Rakowski R. et al. *Appl. Phys. B*, **101**(4), 773 (2010).
24. Fiedorowicz H. et al. *J. Alloys Compd*, **401**(1-2), 99 (2005).
25. Nechay A.N. et al. *Quantum Electron.*, **50**(4), 408 (2020) [*Kvantovaya Elektron.*, **50**(4), 408 (2020)].
26. Wieland M. et al. *Appl. Phys. B*, **72**(5), 591 (2001).
27. Jansson P.A.C. et al. *Rev. Sci. Instrum.*, **76**(4), 043503 (2005).

28. Berglund M. et al. *Rev. Sci. Instrum.*, **69**(6), 2361 (1998).
29. Rymell L., Berglund M., Hertz H.M. *Appl. Phys. Lett.*, **66**(20), 2625 (1995).
30. Malmqvist L. et al. *Rev. Sci. Instrum.*, **67**(12), 4150 (1996).
31. Montcalm C. et. al. *Proc. SPIE*, **3331**, 42 (1998).
32. Polkovnikov V.N. et al. *Phys. Usp.*, **63**(1), 83 (2020) [*Usp. Fiz. Nauk*, **190**, 92 (2020)].
33. Bibishkin M.S. et al. *Nucl. Instrum. Methods Phys. Res. Sect. A*, **543**, 333 (2005).
34. Rebellato J. et al. *Opt. Lett.*, **45**, 869 (2020).
35. Chkhalo N.I. et al. *Appl. Opt.*, **55**(3), 619 (2016).
36. Malyshev I.V., Chkhalo N.I. *Ultramicroscopy*, **202**, 76 (2019).
37. Nechay A.N. et al. *J. Surface Investig.: X-ray, Synchrotron and Neutron Techniques*, **13**, 862 (2019) [*Poverkhnost'. Rentgenovskie, Sinkhrotronnye i Neitronnye Issledovaniya*, **9**, 83 (2019)].
38. Chkhalo N.I. et al. *J. Micro/Nanolithtogr. MEMS MOEMS*, **11**, 021123 (2012).
39. Chkhalo N.I. et al. *Thin Solid Films*, **631**, 106 (2017).
40. Bibishkin M.S. et al. *Proc. SPIE*, **5401**, 8 (2004).
41. Garakhin S.A. et al. *Rev. Sci. Instrum.*, **91**(6), 063103 (2020).
42. Svechnikov M. et al. *J. Appl. Cryst.*, **50**, 1428 (2017).
43. Chkhalo N.I. *Appl. Opt.*, **55**(17), 4683 (2016).
44. Chkhalo N.I. et al. *Thin Solid Films*, **653**, 359 (2018).
45. Aruev P.N. et al. *Quantum Electron.*, **42**(10), 943 (2012) [*Kvantovaya Elektron.*, **42**(10), 943 (2012)].
46. Kelly R.L., Palumbo L.J. *Atomic and Ionic Emission Lines below 2000 Angstroms–Hydrogen through Krypton* (Washington, DC, Naval Research Lab., 1973).
47. Saloman E.B. *J. Phys. Chem. Ref. Data*, **36**(1), 215 (2007).
48. Nechay A.N. et al. *Opt. Spektrosk.*, **129**(3), 266 (2021).
49. Saloman E.B. *J. Phys. Chem. Ref. Data*, **39**(3), 033101 (2010).
50. Nechay A.N. et al. *Opt. Spektrosk.*, **129**(2), 146 (2021).
51. Kalmykov S.G. *Tech. Phys. Lett.*, **35**, 1020 (2009) [*Pis'ma Zh. Tekh. Fiz.*, **35**(21), 97 (2009)].